Supporting Information for Topography dominates the hemispheric asymmetry of Stratospheric Sudden Warmings

Siming Liu[1],Tiffany Shaw[1],Chaim I. Garfinkel[2]

[1]Department of the Geophysical Sciences, The University of Chicago, Chicago, IL

[2]Fredy and Nadine Herrmann Institute of Earth Sciences, The Hebrew University of Jerusalem, Jerusalem, Israel

Contents of this file

1. Figures S1 to S6
2. Topographic Effects on Eddy Heat Flux in a Quasi-Geostrophic Model
3. Figure S10

Introduction

In the Supporting Information, we show details of the simulations which are not shown in the main manuscript.

Corresponding author: Siming Liu, smliu01@uchicago.edu

1. Figures S1 to S6

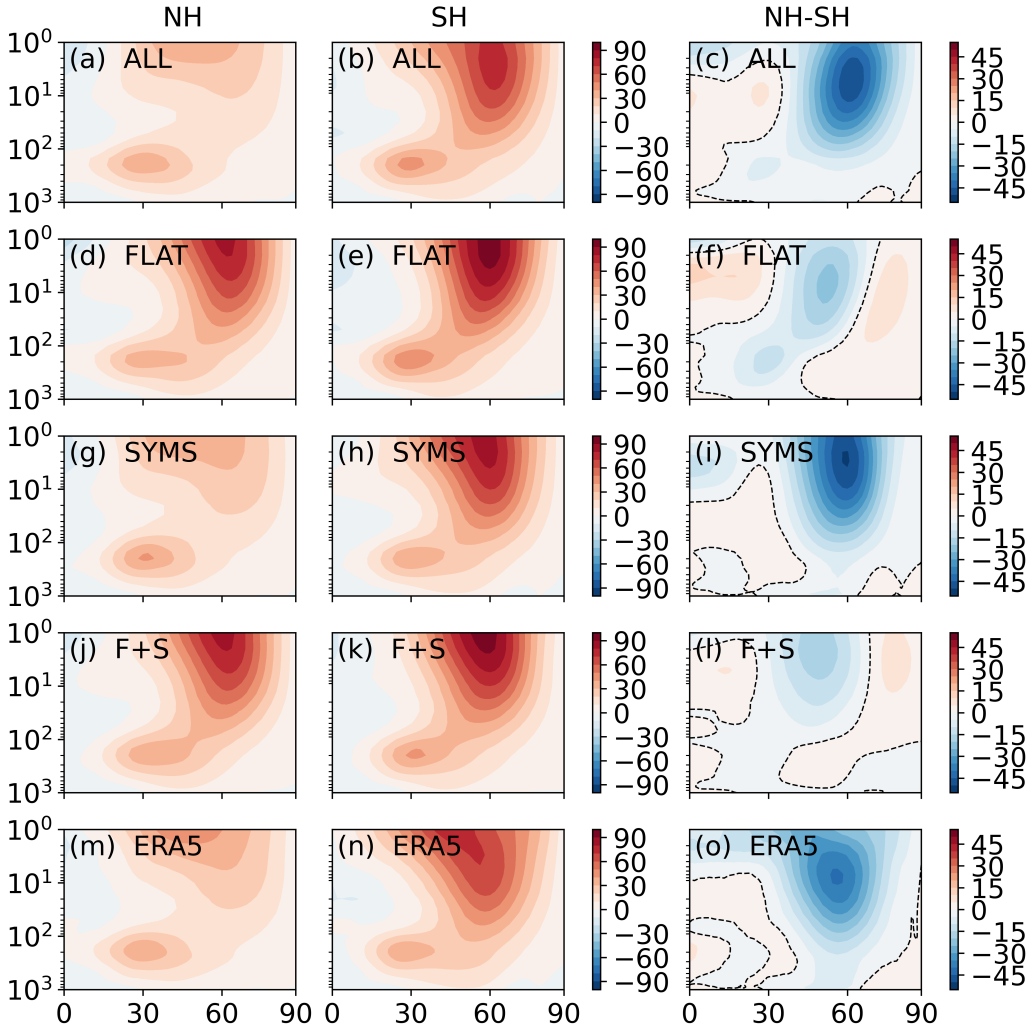

Figure S1. Zonal mean zonal wind ($\overline{u}$, m s^{-1}) in NH (left column), SH (middle column), and the difference between NH and SH (right column) in SSW related season (NH: Nov-Mar, SH: May-Sep) in the climate model forced with observationally derived climatological surface energy fluxes for (a)-(c) climatology (ALL), (d)-(f) flattened topography (FLAT), (g)-(i) symmetrized surface energy fluxes (SYMS), (j)-(l) flattened topography and symmetrized surface energy fluxes (F+S) simulations, and (m)-(o) ERA5 reanalysis.

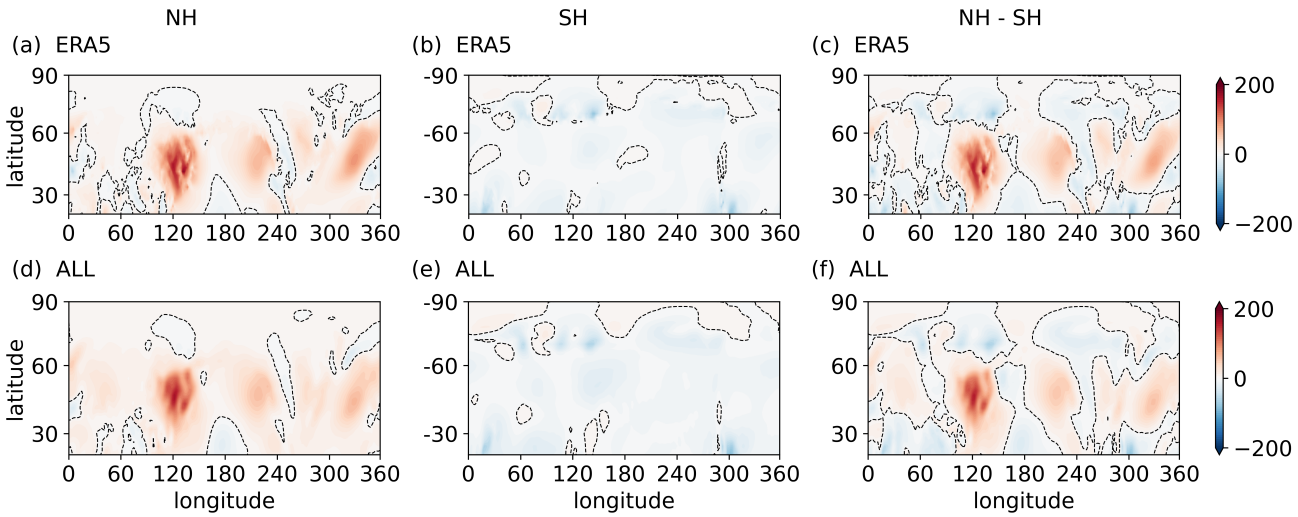

Figure S2. Vertically integrated monthly mean eddy heat flux ($\overline{V^*T^*}$, Km s^{-1}) in (first column) Northern Hemisphere and (second column) Southern Hemisphere in SSW related season (NH: Nov-Mar, SH: May-Sep), and (third column) the difference of the absolute value in Northern and Southern Hemisphere in (a)-(c) ERA5 reanalysis and (d)-(e) the climate model forced with observationally derived climatological surface energy fluxes.

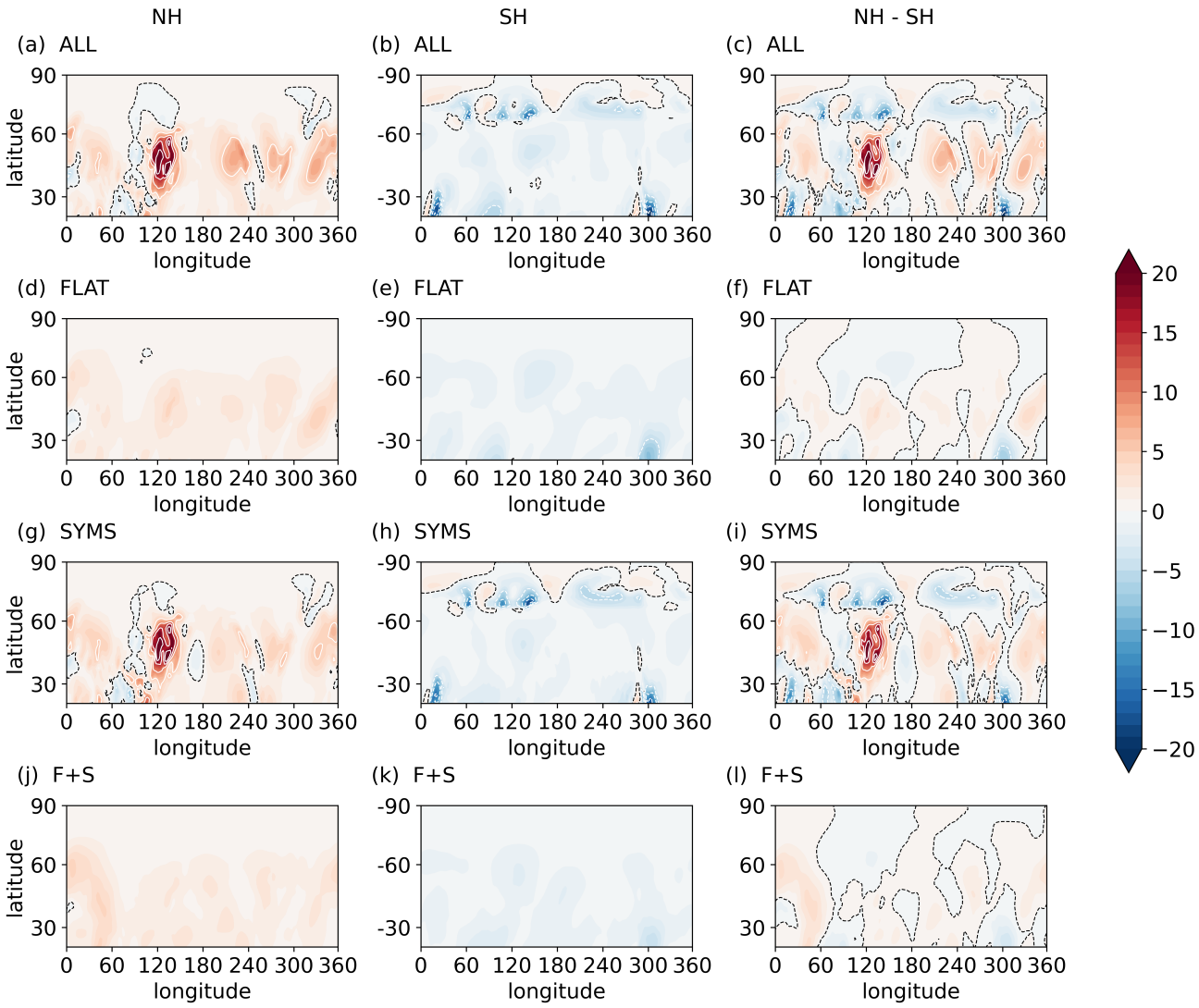

Figure S3. Monthly mean eddy heat flux ($\overline{V^*T^*}$, Km s^{-1}) at 850 hPa in (left column) Northern Hemisphere, (middle column) Southern Hemisphere in SSW related season (NH: Nov-Mar, SH: May-Sep) and (right column) the difference of Northern and Southern Hemisphere in the climate model forced with observationally derived climatological surface energy fluxes for (a)-(c) climatology (ALL), (d)-(f) flattened topography (FLAT), (g)-(i) symmetrized surface energy fluxes (SYMS), and (j)-(l) flattened topography and symmetrized surface energy fluxes (F+S) simulations.

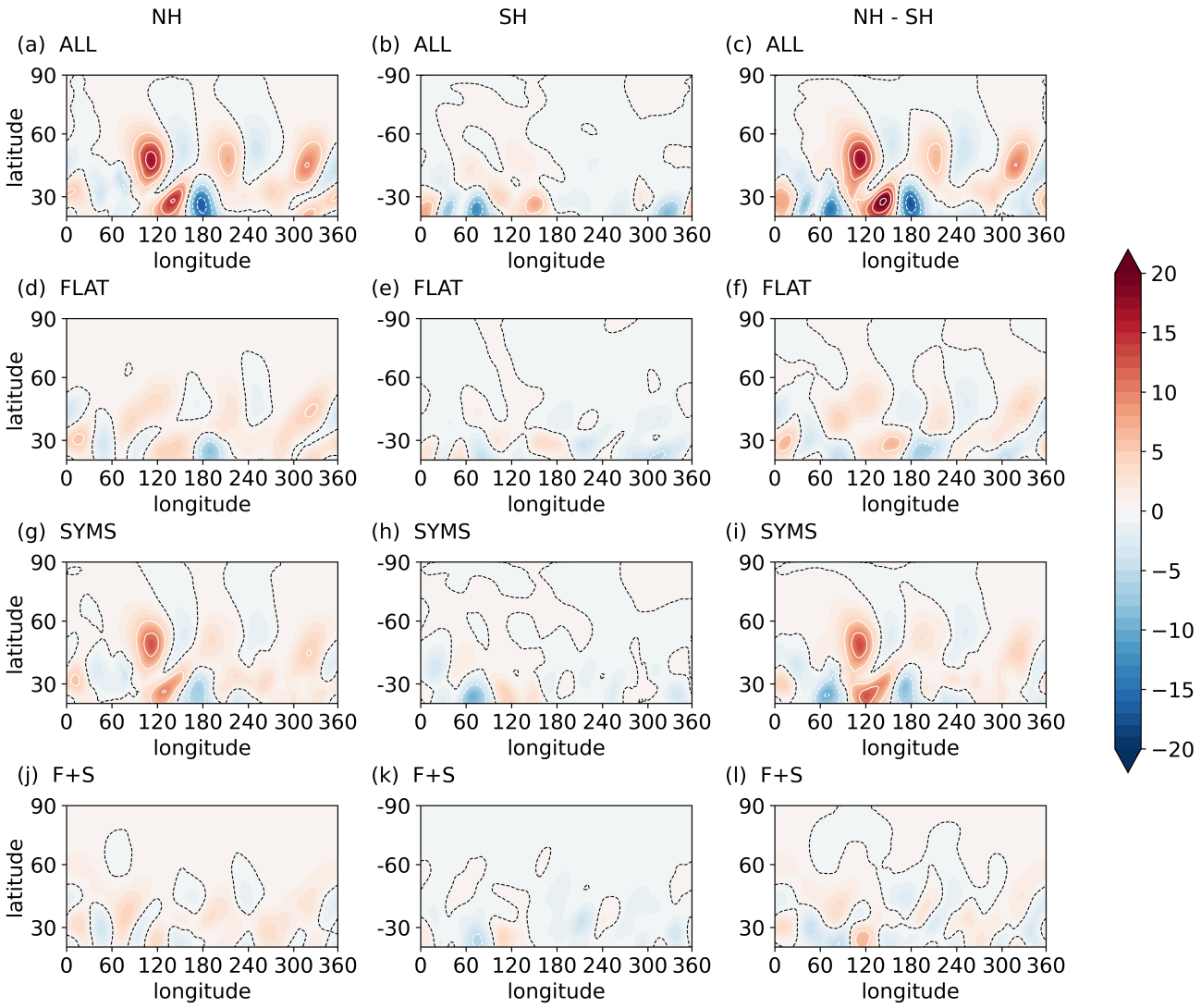

Figure S4. As in Figure S3, but for monthly mean eddy heat flux ($\overline{V^*T^*}$, Km s^{-1}) at 300 hPa.

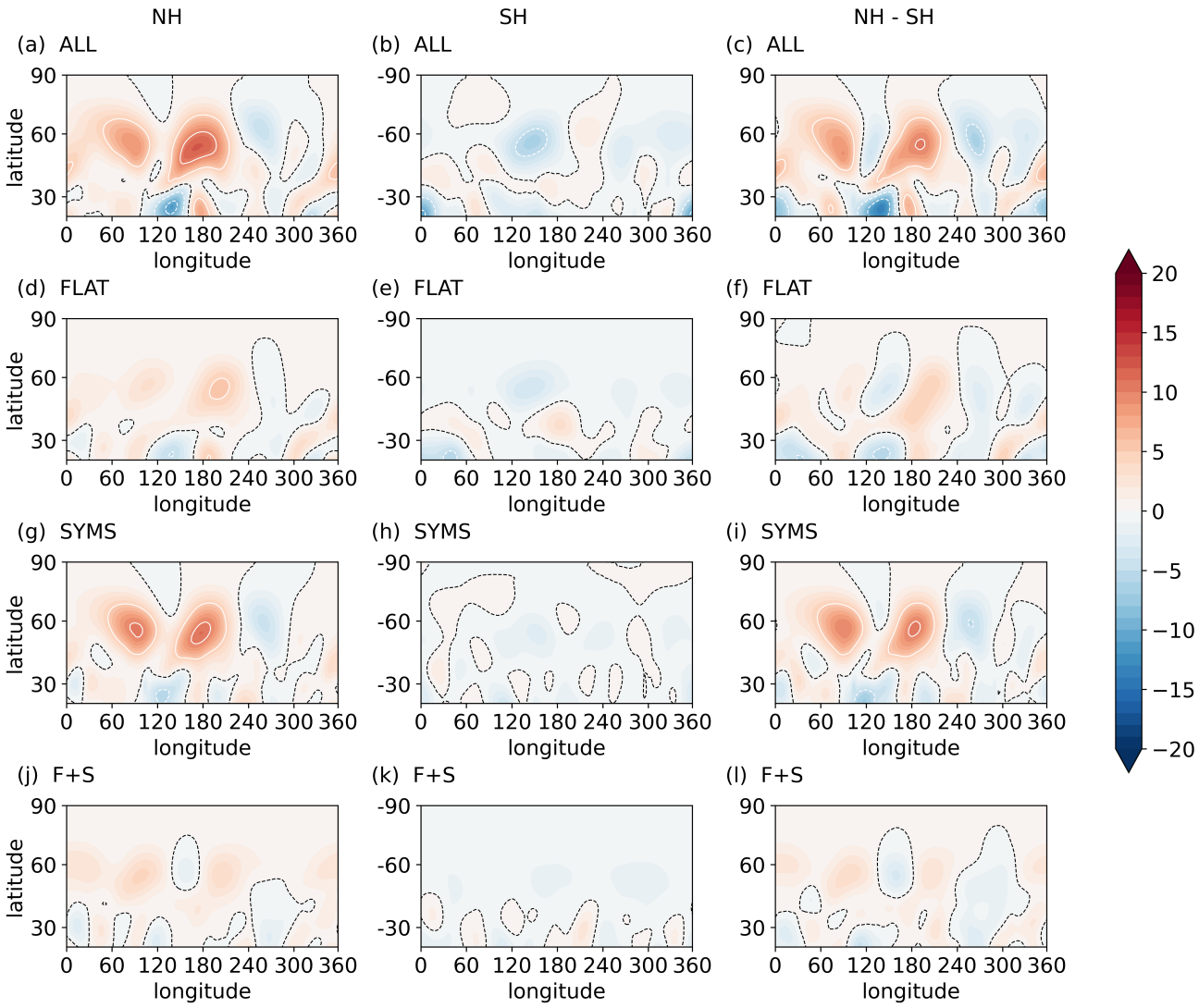

Figure S5. As in Figure S3, but for monthly mean eddy heat flux ($\overline{V^*T^*}$, Km s^{-1}) at 100 hPa.

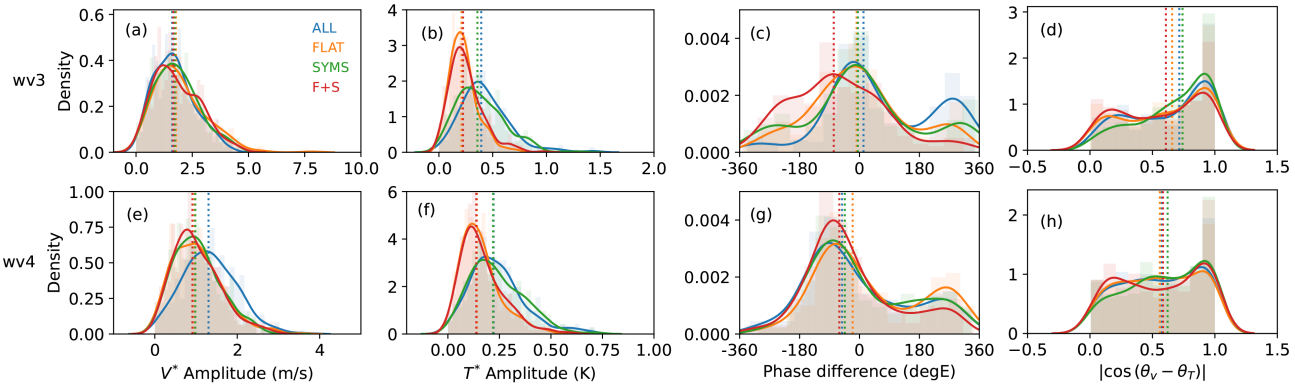

Figure S6. Probability distribution of the amplitude of monthly mean eddy meridional wind (v^*, m s^{-1}) (the first column) and monthly mean eddy temperature (T^*, K) (the second column), the phase difference between the two variables (the third column) and the cosine of the difference between their phases in the NH (the fourth column) for (a)-(d) wave-3 and (e)-(h) wave-4 component at 60°N and 100 hPa in SSW related season (Northern Hemisphere: Nov-Mar) for ALL (blue), FLAT (orange), SYMS (green), and F+S (red) simulations. The dotted lines represents the median value for each distribution.

2. Topographic Effects on Eddy Heat Flux in a Quasi-Geostrophic Model

In order to better understand the effect of topography on eddy heat flux, we use a linear, quasi-geostrophic (QG) β–plane channel model to simulate extratropical planetary wave motions in the middle atmosphere:

$$\left(\frac{\partial}{\partial t} + \bar{u}\frac{\partial}{\partial x}\right) q' + \beta \frac{\partial \psi'}{\partial x} = 0 \tag{1}$$

where

$$q' \equiv \nabla^2 \psi' + \frac{f_0^2}{\rho_0 N^2}\frac{\partial}{\partial z}\left(\rho_0 \frac{\partial \psi'}{\partial z}\right), \qquad \psi = -\bar{u}y + \psi', \qquad \rho_0 \propto e^{-z/H} \tag{2}$$

and H is the scale height. Variable names follow Holton and Hakim (2012). If $\overline{u}$, f_0 and N_0 are all constant, Eq. 1 admits the stationary form of harmonic waves with vertical wave number m:

$$\psi'(x,y,z) = \Psi(z)e^{i(kx+ly)+z/2H}, \qquad \Psi(z) = Ae^{imz}. \tag{3}$$

where k is the zonal wave number, l is the meridional wave number and A is constant.

To simulate a stationary Rossby wave forced by flow over topography, we use the following lower boundary condition on the streamfunction ψ':

$$\frac{\partial \psi'}{\partial z} = -\frac{N_0^2}{f_0}h', \tag{4}$$

where N_0 is chosen as 2×10^{-2} s^{-1}, and h is the topography. For stationary waves,

$$m^2 = \frac{N_0^2}{f_0^2}[\frac{\beta}{\overline{u}} - (k^2+l^2)] - \frac{1}{4H^2}, \tag{5}$$

where $m^2 > 0$ is required for vertical propagation.

We first assume a wavy topography, expressed as

$$h'(x,y) = Be^{i(k_b x + l_b y)}, \qquad z = 0. \tag{6}$$

By Combining (3), (4) and (6), we obtain

$$k = k_b, \qquad l = l_b, \qquad A = -B\frac{N_0^2}{f_0^2}(\frac{1}{2H} + im)^{-1}. \tag{7}$$

Thus, we can derive expressions for eddy meridional wind v^* and eddy potential temperature θ^* as follows:

$$v^* = \frac{\partial \psi'}{\partial x} = -ik_b B\frac{N_0^2}{f_0}e^{z/2H}\left(\frac{1}{2H} + im\right)^{-1} e^{i(k_b x + l_b y + mz)}, \tag{8}$$

$$\theta^* = \frac{f_0\theta_0}{g}\frac{\partial \psi'}{\partial z} = -B\frac{N_0^2\theta_0}{g}e^{z/2H}e^{i(k_b x + l_b y + mz)}. \tag{9}$$

From these, we obtain the magnitude of v^* and θ^*, the eddy heat flux, as well as the cosine of their phase difference:

$$|v^*| = e^{z/2H}\frac{kN_0^2}{f_0}(m^2 + \frac{1}{4H^2})^{-1/2}B, \tag{10}$$

$$|\theta^*| = e^{z/2H}\frac{N_0^2\theta_0}{g}B, \tag{11}$$

$$\overline{v^*\theta^*} = e^{z/H}\frac{km}{2(m^2+\frac{1}{4H^2})}\frac{N_0^4\theta_0}{f_0 g}B^2 = e^{z/H}\frac{km}{2(\frac{\beta}{\overline{u}}-k^2-l^2)}\frac{N_0^2 f_0\theta_0}{g}B^2, \tag{12}$$

$$\cos(\phi_v - \phi_\theta) = \frac{\overline{v^*\theta^*}}{|v^*||\theta^*|} = \frac{m}{2(m^2+\frac{1}{4H^2})^{1/2}} = \frac{mf_0^2}{2N_0^2(\frac{\beta}{\overline{u}}-k^2-l^2)}. \tag{13}$$

From the equations above, it is clear that the magnitudes of v^* and θ^* are both proportional to the magnitude of the topography B; thus, an increase in topography leads to a corresponding increase in their magnitudes. The amplitude of v^* is greater for wave 2 than for wave 1 (Fig. S7a), which is consistent with what is seen in the climate model simulations (Fig. 4a, e), where the wave-1 and wave-2 components of topography exhibit comparable amplitudes in reality.

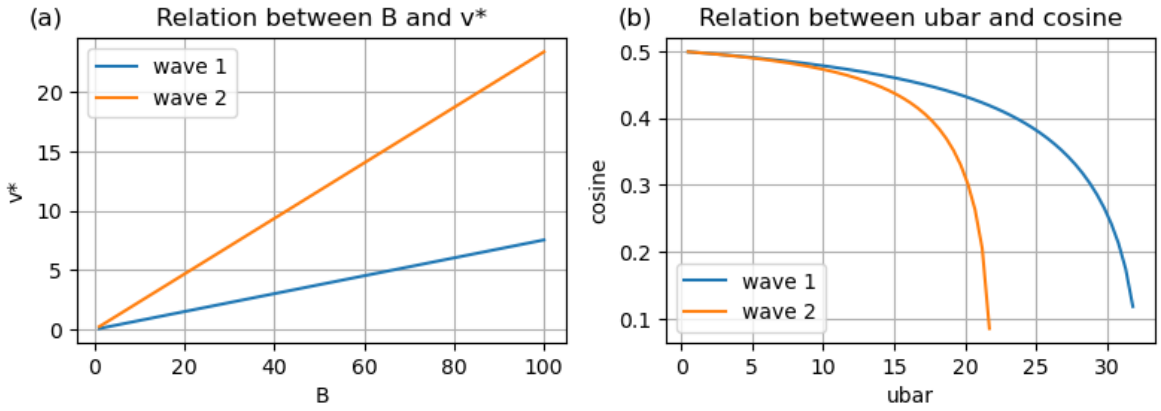

Figure S7. The relation between (a) the magnitude of topography B and eddy meridional wind v^*, and (b) the zonal mean zonal wind $\overline{u}$ and the cosine of the phase difference in linear QG theory.

The cosine of their phase difference is dependent on m, which in turn is influenced by the zonal mean zonal wind $\overline{u}$. As the amplitude of topography increases, the upward E-P flux also

increases ($F_z = \frac{f_0}{\partial\overline{\theta}_0/\partial z}\overline{v^*\theta^*}$), which enhances wave activity. By wave–mean flow interaction, this leads to a reduction in the zonal mean wind. When the zonal wind decreases, the cosine of the phase difference increases for both wave numbers (Fig. S7b), with a greater increase for wave 2, consistent with the climate model simulation results (Fig. 4d, h).

We also utilize 60 years of 6-hourly winter $\bar{u}$ data (Nov-Mar) from ECHAM6 ALL simulation at each altitude as input to the QG model. The model is forced by two different topographical scenarios: one with realistic topography across 30°-60° N in the NH from the ALL simulation (Fig. S8a, red), and the other with smoothed topography across 30°-60° N in the NH, serving as a comparison to simulate a flattened topography scenario (Fig. S8b, blue). The model generates the time-height evolution of meridional velocity v and temperature T.

Figure S8a, b presents the eddy meridional wind and eddy temperature climatology for realistic and smoothed topography. The comparison reveals that realistic topography leads to more pronounced and complex circulation patterns, while smoothed topography produces a more uniform flow, which highlights the impact of topography on the atmospheric circulation. The response to flattening topography in the conceptual model is similar to that observed when comparing the ALL (Fig. S10a) and FLAT (Fig. S10b) simulations. A phase mismatch occurs between the QG model (Fig. S8) and the ECHAM6 model (Fig. S10) starting at the surface. This likely results from factors the QG model cannot account for, such as land-sea contrasts and oceanic heat fluxes, making a perfect phase match with General Circulation Models unrealistic. However, the QG model is still useful for demonstrating how topography increases the cosine of the phase difference between the meridional wind and temperature.

Fig. S8 also shows the probability distributions of the amplitude and phase difference of the monthly mean eddy meridional wind and eddy temperature at 100 hPa and 60°N for the β-plane

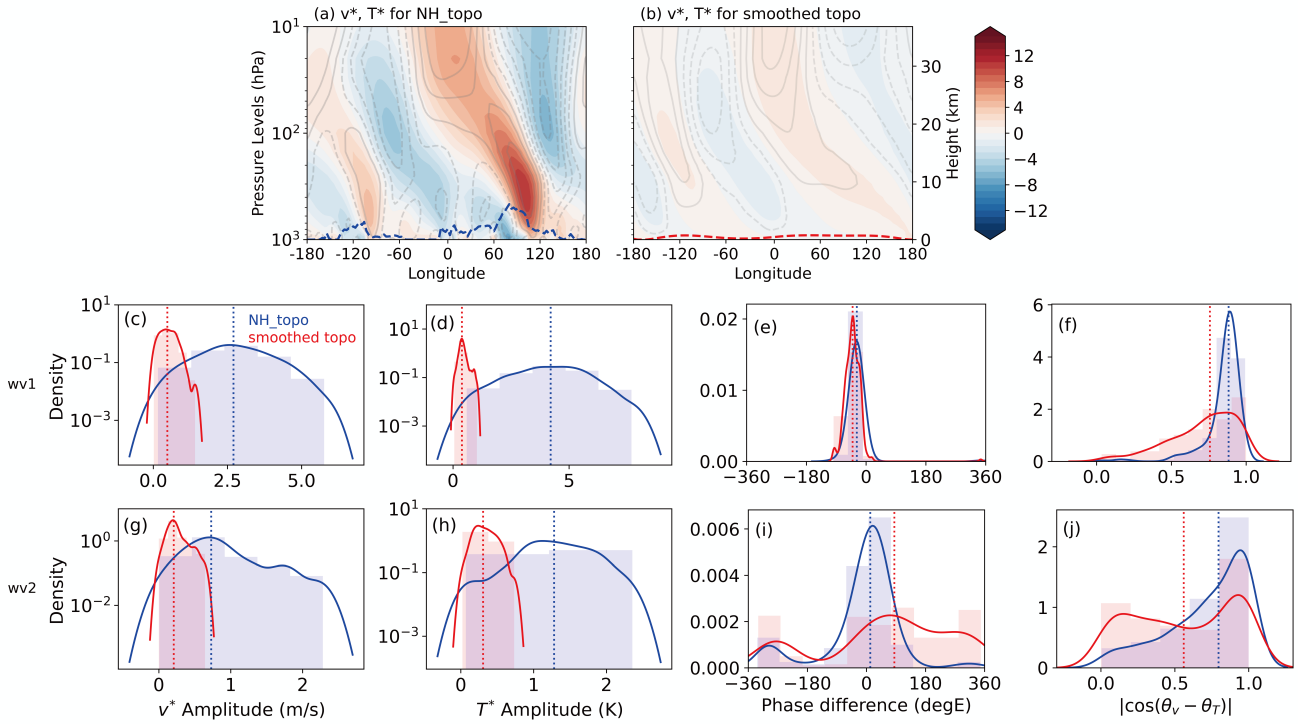

Figure S8. Meridional wind (v, gray dashed line) and temperature (T, shading) climatology over 60 years of simulation (shading) for the β-plane channel model with (a) realistic and (b) smoothed topography across the NH. The black dashed line indicates the 0 value, the red dashed line represents the realistic topography, and the blue dashed line represents the smoothed topography. (c)-(j) As in Figure 4, but for the realistic topography forced (red) and smoothed topography forced (blue) simulations.

channel model with realistic and smoothed topography. Similar to the FLAT model simulation, smoother topography results in a decrease in the median value of the wave amplitude for both eddy meridional wind (Fig. S8c, g) and eddy temperature (Fig. S8d, h). Additionally, smoothing the topography results in a decrease in the cosine of the phase difference for both wave-1 (Fig. S8f) and wave-2 (Fig. S8j). The probability distribution of the cosine of the phase difference shifts toward 0 due to the deviations of phase difference from 180° out of phase (Fig. S8e, i).

Although the results differ somewhat from those in Fig. 4, likely due to the β-plane channel model's limitations in capturing higher-order dynamics, the overall impact of topography on eddy behavior aligns with the findings from climate model simulations.

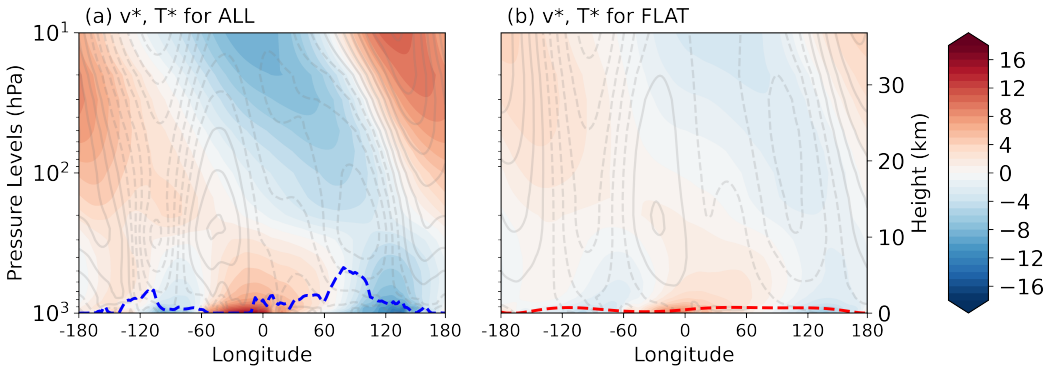

Figure S9. Eddy meridional wind (v^*, gray lines) and eddy temperature (T^*, shading) climatology in Nov-Mar at 60°N over 60 years of simulation for (a) ALL and (b) FLAT simulations. The blue dashed line represents the realistic topography, and the red dashed line represents the smoothed topography.

Several factors related to atmospheric wave propagation and wave-mean flow interactions may contribute to why smoother topography can cause the eddy meridional wind (v^*) and eddy temperature (T^*) fields to become more out of phase (cosine less than 1). Smoothing the topography can weaken the generation of stationary waves and reduce the amplitude and coherence of eddies, leading to less organized wave structures and a diminished phase coupling between v^* and T^*. Additionally, strong topography enhances wave-mean flow interactions, which tend to strengthen specific phase relationships. When the topography is flattened, these interactions are reduced, allowing the two fields to behave more independently, potentially resulting in a phase shift. Overall, the combined effects of weaker wave structures, reduced interactions, and diminished eddy coherence contribute to a more pronounced phase difference between v^* and T^*.

3. Figure S10

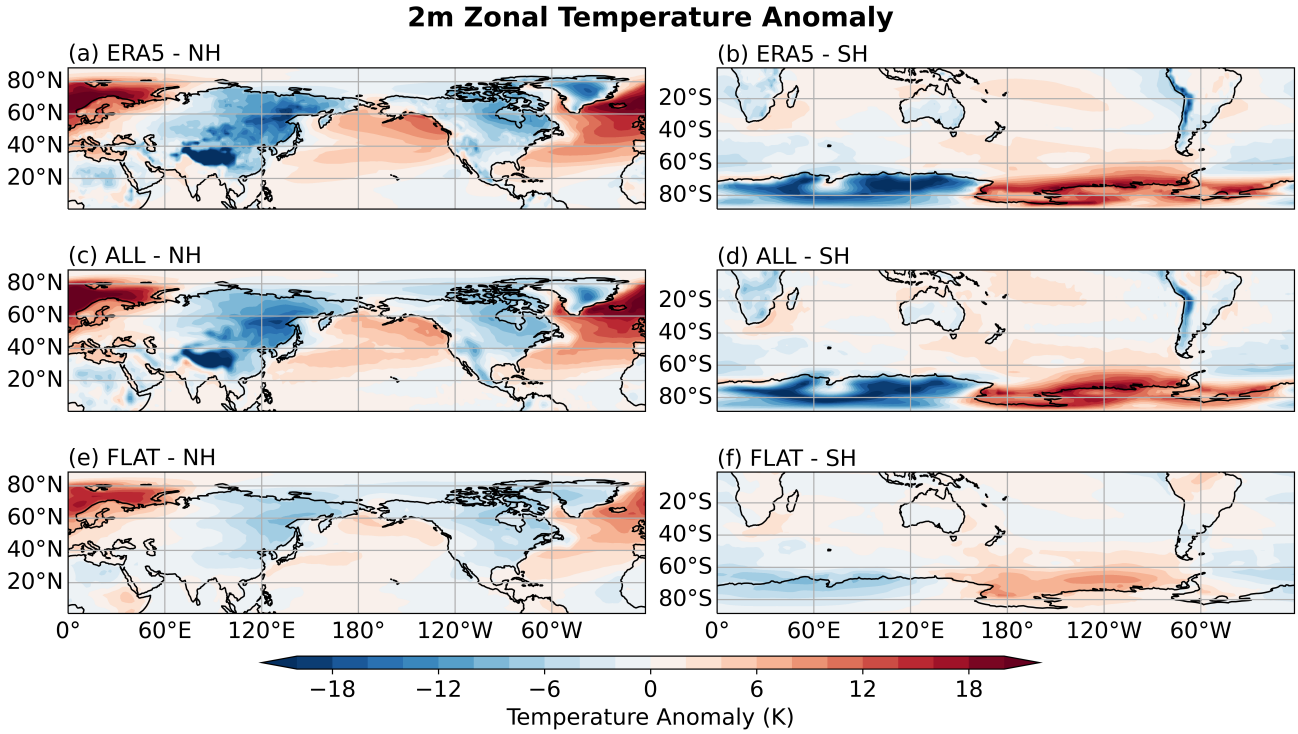

Figure S10. Zonal temperature anomaly at 2 meter in NH (left column) and SH (right column) in SSW-related season (NH: Nov-Mar, SH: May-Sep) in (a)-(b) ERA5 and the climate model forced with observationally derived climatological surface energy fluxes for (c)-(d) climatology (ALL), (e)-(f) flattened topography (FLAT) simulations.

References

Holton, J. R., & Hakim, G. J. (2012). *An introduction to dynamic meteorology* (5th ed.). Cambridge, MA: Academic Press.